Optimum Design of an Aircraft-Mounted Pod for Improved Aero-Optic Performance

Grady Crahan,[1] Mark Rennie,[2] Eric J. Jumper,[3] Andrés Tovar,[4] Gilberto Mejía-Rodríguez,[5] and John E. Renaud[6]
Department of Aerospace and Mechanical Engineering, University of Notre Dame, Notre Dame, IN, 46556

Aero-optic aberrations originating from the nearby flowfield of an aircraft can seriously limit the ability to focus on-board laser systems onto farfield targets. These aero-optic aberrations can be mitigated by using fences to control the flow around the outgoing beam aperture. The objective of this investigation is to attempt to determine the best shape for these fences using computational fluid dynamics in combination with optimization techniques. Future work will experimentally and computationally build on the solutions presented here.

Nomenclature

a_j	=	parameters from fitting polynomial function
C_P	=	pressure coefficient
C_{P0}	=	pressure coefficient in incompressible flow
M	=	local Mach number
M_∞	=	freestream Mach number
D	=	pod turret diameter
h	=	height of the fence
x	=	axial position
x_D	=	normalized axial position (x/D)
x_1	=	normalized position x_D where the fence begins
x_2	=	normalized position x_D to farthest point from the centerline to the fence
y	=	radial transverse position
y_D	=	normalized radial transverse position (y/D)
y_1	=	normalized position y_D where the fence begins
y_2	=	normalized position y_D to farthest point from the centerline to the fence
z	=	radial normal position
θ	=	lookback angle
θ_r	=	ramp angle
γ	=	ratio of specific heats (air = 1.4)

I. Introduction

AN aircraft traveling at compressible flow speeds is surrounded by optically-active regions which are formed by high density and associated index-of-refraction gradients.[1] These optically-active regions originate from localized compressible turbulent flowfields or inviscid flows such as shock waves.[2] The aberrations produced by these optically-active regions can have disastrous consequences for a traversing beam of light, and so can significantly restrict the effective field of regard of optical systems carried by the aircraft.

A possible mitigation approach to aero-optic flows is to employ an adaptive-optic (AO) system[3] that places the conjugate waveform of the aberration onto the wavefront of the beam prior to its transmission through the aberrating

[1] Graduate Research Assistant, Center for Flow Physics and Control, AIAA Student Member, gcrahan@nd.edu.
[2] Research Assistant Professor, Center for Flow Physics and Control, AIAA Member, rrennie@nd.edu.
[3] Professor, Center for Flow Physics and Control, AIAA Fellow, ejumper@nd.edu.
[4] Research Assistant Professor, Design Automation Laboratory, AIAA Member, atovar@nd.edu.
[5] Graduate Research Assistant, Design Automation Laboratory, AIAA Student Member, gmejiaro@nd.edu.
[6] Professor, Design Automation Laboratory, AIAA Fellow, jrenaud@nd.edu.

flowfield; contemporary AO systems are unable, however, to match the high temporal frequencies associated with aero-optic flows. Flow-control approaches that attempt to modify the local boundary layer using, for example, pins or vortex generators to delay separation and thus reduce the size of the optically-active region have also met with limited success[4], and neither AO or flow-control approaches address the aero-optic problem presented by shock waves. The difficulties associated with these approaches suggest that considerable advantage could be gained by careful aerodynamic design of the mounting arrangement for the optical system that avoids the formation of strongly-aberrating flow regions in the first place. The objective of this investigation is to optimally design the shape of an aircraft-mounted laser pod in order to minimize aero-optic aberrations.

II. Basic Design Concept

Probably the simplest solution to providing control over the azimuth and elevation of an optical system is to mount the system in a spherical turret. It has been shown, however, that spherical turrets generate local supersonic flows at flight speeds that are well below typical cruise speeds for jet fighters or transport aircraft[5]; the resulting supersonic flow region terminates in a shock wave that can seriously degrade the optical properties of a laser beam that passes through it. Spherical turrets are also susceptible to boundary-layer separation from their leeward surfaces; at compressible flow speeds, the shear layer associated with the resulting separated flow region downstream of the turret becomes optically active in the sense that vortical structures within the shear layer produce severe gradients in the density and hence index of refraction[4.1]. In Ref. 5, we presented a concept for the mitigation of the aero-optic effects associated with spherical turrets, by mounting carefully-shaped fences to the surface of the turret; this concept is briefly reviewed in the following sections.

A. Geometric Layout

In incompressible flow, the peak negative C_{P0} on the surface of a spherical turret is -1.25, and occurs on the top of the turret. This C_{P0} can be corrected for compressibility effects using, for example, the Karman-Tsien correction, which is given by

$$C_P = \frac{C_{P0}}{\sqrt{1-M_\infty^2} + \frac{C_{P0}}{2}\left(1-\sqrt{1-M_\infty^2}\right)}. \tag{1}$$

Similarly, the critical Mach number can be expressed as

$$C_{Pcrit} = \frac{2}{\gamma M_{crit}^2}\left[\left(\frac{1+\frac{\gamma-1}{2}M_{crit}^2}{1+\frac{\gamma-1}{2}}\right)^{\frac{\gamma}{\gamma-1}} - 1\right]. \tag{2}$$

From the intersection of Equations (1) and (2), shock formation occurs on a spherical turret at a Mach number just below 0.53 (Figure 1). This value is significantly below the nominal M ≈ 0.8 cruise speed of jet transports and combat aircraft. .

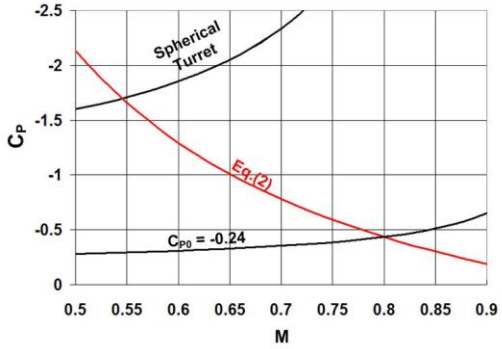

Figure 1. Critical Mach number for spherical turret, and minimum C_P for cruise at M = 0.8.

As shown by Fig. 1, in order to avoid shock formation up to M ≈ 0.8, the local minimum C_{p0} in the region of interest must be approximately -0.24 or greater. One method of achieving this target would be to streamline the spherical turret using an appropriately shaped fairing. A fairing shape with a "cubic forebody" (i.e. with $y = ax^3 + bx^2 + cx + d$) that achieves subsonic flow around the aperture is shown in Figure 2. The figure also shows an illustration of an axisymmetric "pod" (such as would be mounted externally to an aircraft) based on the cubic forebody. The optical aperture is located on the spherical turret ball at the front of the pod. To increase the aft field of regard, the pod has a cutout that enables the turret ball to rotate the aperture to rearward look-back angles. A "roll shell" that contains the turret ball and cutout is used to rotate the aperture in the azimuthal direction.

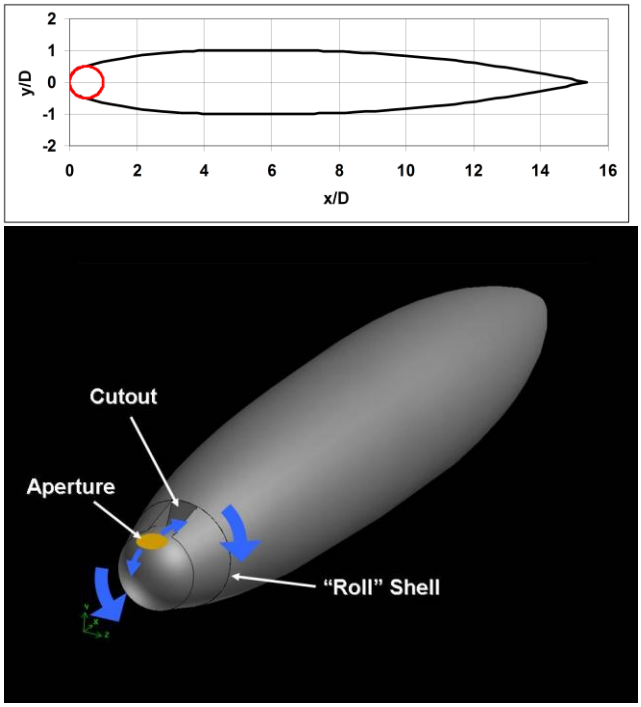

Figure 2. Cubic forebody fairing shape in 2-D (above) and 3-D (below). The turret ball is shown as the red circle at the nose of the front of the pod.

B. Cutout

In Figure 2, the cutout that enables the aperture to rotate to aft pointing angles has simple, straight walls that are separated by the aperture diameter so that the edges of the aperture will not be obscured by the pod. Computational fluid dynamics (CFD) results show, however, that the critical Mach number for this "simple" cutout design is significantly lower than the $M = 0.8$ target. Investigations have shown that the straight walls of the cutout cause this reduction in critical Mach number. As shown in Figure 3, these straight walls constrict the streamlines over the top of the turret ball, which normally follow "lines of longitude" along the spherical surface of the turret ball. This streamline constriction results in increased flow speeds over the top of the ball and the observed reduction in critical Mach number. The straight cutout walls also diffuse the flow on the back of the ball faster than if the flow followed lines of longitude on the ball surface; this higher diffusion increases the adverse pressure gradient on the back of the turret ball thereby increasing the risk of flow separation and associated aero-optic aberrations. As illustrated in Fig. 4, these effects can be counteracted by shaping the cutout walls to diffuse the flow at the front of the turret ball, and contract at the back of the ball. The effectiveness of the cutout walls can be enhanced by extending the walls into the flow with a "fence." An example of a fairing with an improved cutout shape that implements these ideas is shown in Fig. 5.

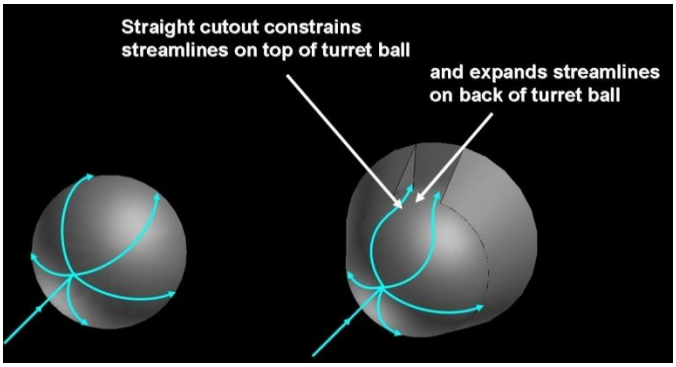

Figure 3. Illustration showing how straight cutout walls constrain streamlines on the turret ball

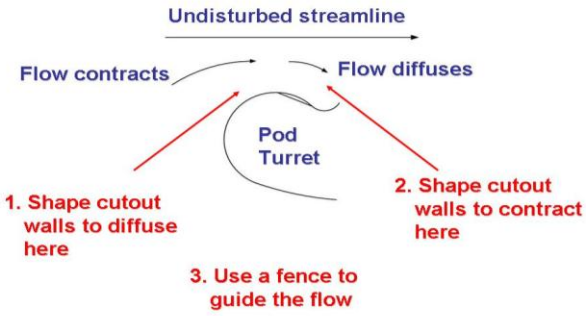

Figure 4. Diagram showing how cutout wall shaping can improve the flow, and aero-optic environment around the turret ball.

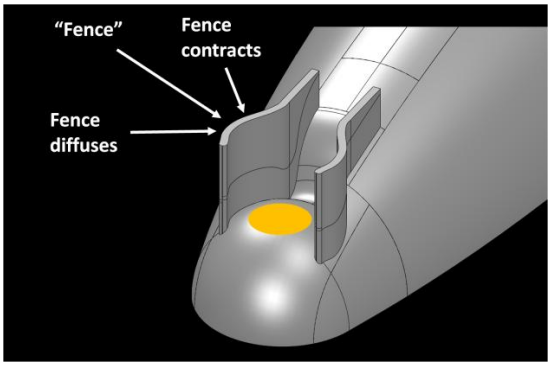

Figure 5. Top part of pod with improved cutout and fence to control flow around aperture.

Pressure distributions computed using CFD for the original fairing shape, the fairing with simple straight-wall cutout, and the fairing with improved cutout are shown in Figure 6. The figure shows that the critical Mach number for the fairing with the improved cutout is even higher than for the unmodified shape (M = 0.86 versus M = 0.8). Further, the adverse pressure gradient on the back of the turret ball has also been reduced, which alleviates the possibility for flow separation and concomitant strong aero-optic aberrations at large look-back angles.

Further CFD studies were also completed using different heights for the fences and different lookback angles. Figure 7 shows the centerline geometry of 3 different lookback angles that were tested. Figure 8 shows the C_{p0} data for different lookback angles at two different fence heights. It is shown that the M_{crit} = 0.8 design objective can be attained for the 40° lookback case and nearly for the 60° case, although increasing the fence height beyond the tested range may increase the achievable critical Mach number still further.

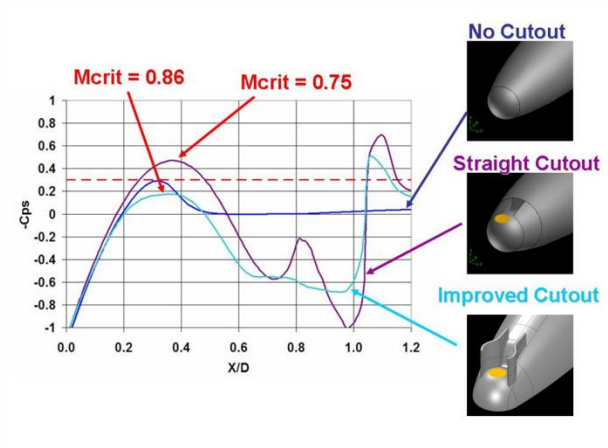

Figure 6. CFD-computed pressure distributions around turret ball and critical Mach numbers for different cutout configurations at 20 degree lookback.

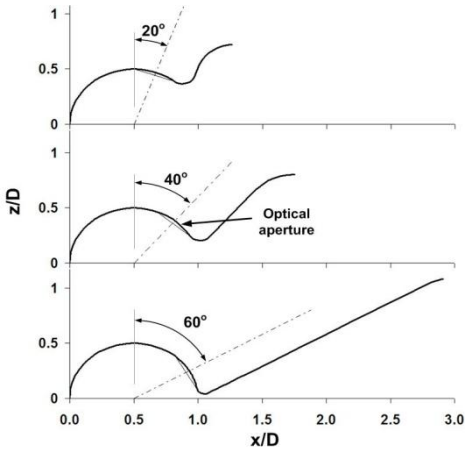

Figure 7. Centerline geometry for different lookback angles.

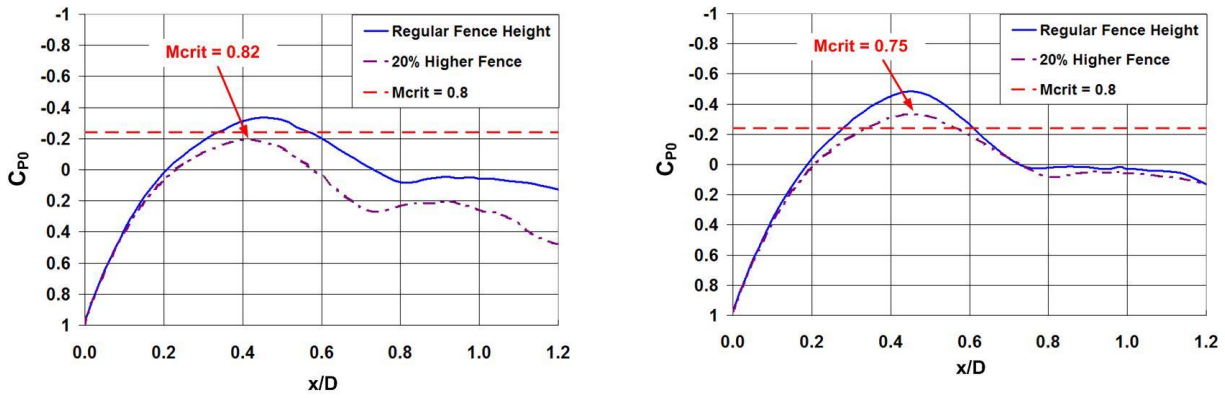

Figure 8. CFD-computed pressure distributions around turret ball for 2 different fence heights at a lookback angle of 40 degrees (left) and 60 degrees (right).

III. Optimization Approach

The CFD data shown Figs. 6 to 8 show how a fence design developed in a trial-and-error fashion can significantly improve the critical Mach number and boundary-layer separation performance of a spherical turret. There is, however, no guarantee that the design that produced the significantly-improved results shown above was an optimum, or even nearly-optimum design, and that even better performance cannot be achieved. Considering the basic fence concept shown in Fig. 5, it is clear that there are a multitude of possible fence designs that would result in an improvement over the unmodified hemispherical turret design. The following describes the systematic optimization approach that was employed in an attempt to arrive at the optimum fence design.

In order to develop and verify the methodology, optimization was first attempted on a simplified model, consisting of a hemispherical turret on a D/3 cylindrical base (Fig. 9). The hemisphere-on-cylindrical-base turret is a very commonly used turret configuration[4], so that results obtained in this initial work will have immediate application; however, the simplicity of the geometry means that computational model sizes can be kept small, making it possible to perform optimizations with reduced computational expense.

Several optimization techniques have been developed to solve computationally-expensive problems. For example, successive approximation techniques have been used to reduce computational cost, especially when the sampling needed to create the response surface is on the order of the number of design variables.[6,7] Other techniques, based on the variable-fidelity optimization framework, have been used in application to the design of a high-lift airfoil, to find the optimal placement of its slat, vane, and flap to provide maximum lift for takeoff or landing, and in application to design of complex nanomaterials.[8, 9] Shape optimization is a computational-based approach in which the objective is to determine the optimal profile or boundary of the structure. Two of the most common approaches to performing shape optimization are the *basis vector* and the *grid perturbation* approach. The basis vector approach

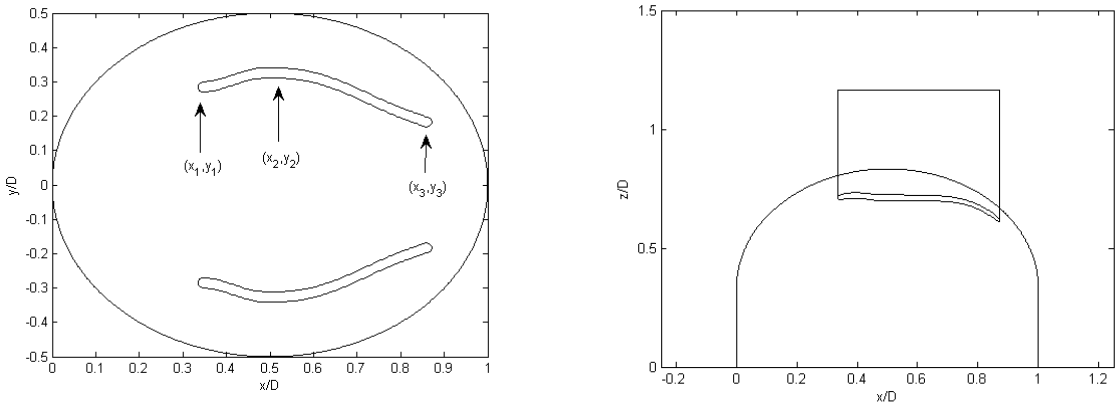

Figure 9. Top (left) and side (right) view of turret with flow in positive x-direction.

requires the definition of different trial designs called basis vectors. The design variables are the weighting parameters that define the participation of each basis vector in the design process. On the other hand, the grid perturbation approach requires the definition of perturbation vectors. These vectors perturb or deform the boundary of the design domain. The design variables are the values that determine the amount of perturbation during the optimization process. This investigation will implement a classical shape optimization algorithm based on grid perturbation.

A. Objective function

The objective is to minimize optically-active flows around a spherically-shaped turret, where the two main causes of optical aberrations for this case are shock waves and flow separation. As discussed above, shock formation on the turret can be avoided by keeping the minimum C_{P0} on the turret as large as possible. On the other hand, treatment of the no-separation criterion is more difficult, since ideally the optimization approach should allow the use of "low-fidelity" analysis routines, such as an inviscid-Euler routine, that cannot directly predict boundary-layer separation. It is well known, however, that the chance of boundary-layer separation increases when a strong adverse pressure gradient exists in the region of interest; as such, the no-separation objective was modeled by minimizing the adverse pressure gradient over a selected region of the rear of the turret. This region was chosen to begin at x/D = 0.4 (see Fig. 9), and to extend sufficiently far downstream to enable a maximum lookback angle of 40^o; for a typical turret design in which the aperture is $1/3^{rd}$ the diameter of the turret, Figure 10 shows that this criterion means that flow separation must be prevented (as far as possible) up to x/D = 0.91. It should be noted that the maximum lookback angle of 40^o was chosen arbitrarily; however, since flow separation on a spherical turret normally occurs at only 30^o past vertical, Fig. 10 shows that maintaining flow separation over the range x/D = 0.4 to 0.91 would represent a significant improvement over the normal case.

Based on the above discussion, the objective function can be expressed as

$$\min_{0.4\le\frac{x}{D}\le 0.91} \sum \left\{ \left| \frac{d}{dx} C_P\left(\frac{x}{D}\right) \right| \right\} \tag{3}$$

where C_P is the pressure coefficient. For the CFD data at discrete points x_i/D, the objective function can be written as

$$\min_{0.4\le\frac{x_i}{D}\le 0.91} \sum \left\{ \left| \frac{C_P\left(\frac{x_i}{D}\right) - C_P\left(\frac{x_{i-1}}{D}\right)}{x_i - x_{i-1}} \right| \right\}. \tag{4}$$

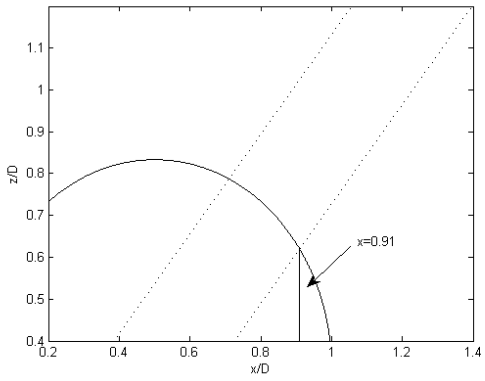

Figure 10. Side view of turret with the laser at lookback angle of 40 degrees.

For this initial application, the flow was solved using only the low-fidelity inviscid Euler equations. In future research variable-fidelity optimization will be investigated in which the flow will also be periodically solved using a higher-fidelity model such as the full Navier-Stokes equations.

B. Design variables

The fence wall coordinates were determined using fifth-order polynomials for both the diffusing and contracting sections; fifth-order polynomials are often used for wind-tunnel contraction design.[9.1] As such, fence shapes could be fully determined by specifying the locations of the points 1, 2, and 3 shown in Fig. 9, plus the boundary conditions of zero slope and curvature at the start and end of each section of the fence. Furthermore, since the streamlines normally follow "lines of longitude" on the hemispherical surface of the turret, the fence coordinates were

defined with respect to lines of longitude rather than with respect to the oncoming flow. The objective of the initial work was to optimize the shape of the fence by determining the optimum locations of the points 1, 2 and 3 shown in Fig. 9. It is known that higher fence heights increase the critical Mach number;[5] therefore, h was set to a constant. In summary, six design variables were used: x_1, y_1, x_2, y_2, x_3, and y_3.

C. Constraints

The main constraint on the system is the lower limit on the pressure coefficient; as shown above, to obtain a critical Mach number, M_{crit}, of 0.8, the C_{P0} must be -0.24. For this initial investigation, however, the constraint on minimum C_{P0} was relaxed to -0.5. Geometric constraints on the reference points of the fence were also imposed to avoid fence shapes that would lie on the optical aperture of the turret. For this constraint, all points on the fence must have a coordinate y that is greater than or equal to $0.17D$ away from the centerline of the pod (again, assuming a typical turret configuration with an aperture diameter that is 1/3rd the diameter of the turret). Other constraints included an upper limit on the y coordinates of the fence of 0.45 D, and x coordinates between 0 and D. Finally, the fence thickness was set to to 0.03 D:

$$\sqrt{(x_i - 0.5)^2 + y_i^2} \leq 0.45 \quad \text{for i = 1, 2, 3,}$$

$$0 \leq x_i \leq 1 \quad \text{for i = 1, 2, 3, and}$$

$$0.17 \leq y_i \leq 0.45 \quad \text{for i = 1, 2, 3.}$$

A further constraint on the system is to make sure that no point overlaps or gets too close to another point, eg. point 2 must be located further downstream than point 1. The optimization problem in standard form can be stated as follows:

$$\min_{0.4 \leq x \leq 0.91} \Sigma \left\{ \left| \frac{\Delta C_{p_i}}{\Delta x_i} \right| \right\}$$

$$\text{s.t.} \quad -(min(C_p)) \leq 0.5 \,,$$

$$x_1 - x_2 \leq -0.1,$$

$$x_2 - x_3 \leq -0.1,$$

$$y_1 - y_2 \leq -0.015,$$

$$y_3 - y_2 \leq -0.015,$$

$$\sqrt{(x_i - 0.5)^2 + y_i^2} \leq 0.45 \quad \text{for i = 1, 2, 3,}$$

$$0 \leq x_i \leq 1 \quad \text{for i = 1, 2, 3, and}$$

$$0.17 \leq y_i \leq 0.45 \quad \text{for i = 1, 2, 3.}$$

D. Methodology for Design Optimization

This problem is defined for a non-linear and computationally expensive objective function and a set of linear (geometric) constraints. The approach is based on the sequential quadratic programming (SQP)[10] method. The quadratic approximation of the objective function, subject to the set of linear constraints, is solved with an active-set approach[11] in order to find a search direction at each iteration. The step size is obtained by solving a penalized single-variable optimization problem.[12]

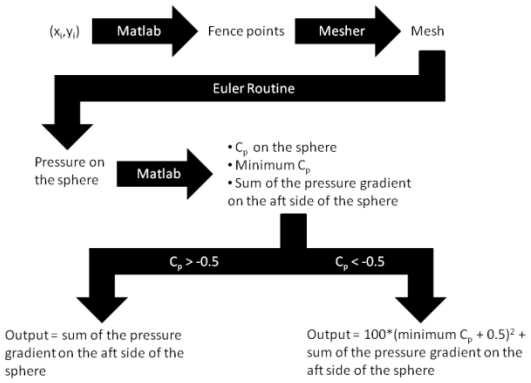

Figure 11. Flow chart of function call

The Matlab function, fmincon, was used along with the constraints above and the active-set algorithm. A function call was written that calls the various meshing and CFD routines in an automated c-script. Fig. 11 shows this process in a flow chart starting with the input points and proceeding to the output. Starting at the beginning, the three points from Figure 9 that define the fence constitute the input to the function call. Once the fence coordinates are determined, the mesh is generated and solved by the CFD routine. The minimum C_{P0} on the sphere along with the sum of the pressure gradient are then evaluated to determine if the new point is feasible or not. To take into account the constraint on C_{p0}, a penalty is incorporated into the function call. by using an " if " statement that looks at the pressure value; if it is below the constraint, it will take the distance away and multiply it by a penalty factor of 100. This penalty is then added to the function value.

IV. Results

The optimization problem formulated in the preceding section was investigated by computing the value of the objective function, Eq. (4), over a reasonable range of positions for the fence points 1, 2, and 3 (Fig. 9). Noting that the objective function shown in Eq. (4) evaluates the adverse pressure gradient on the rear of the turret, this exercise effectively demonstrates how the fence shape influences the chance of boundary-layer separation from the turret.

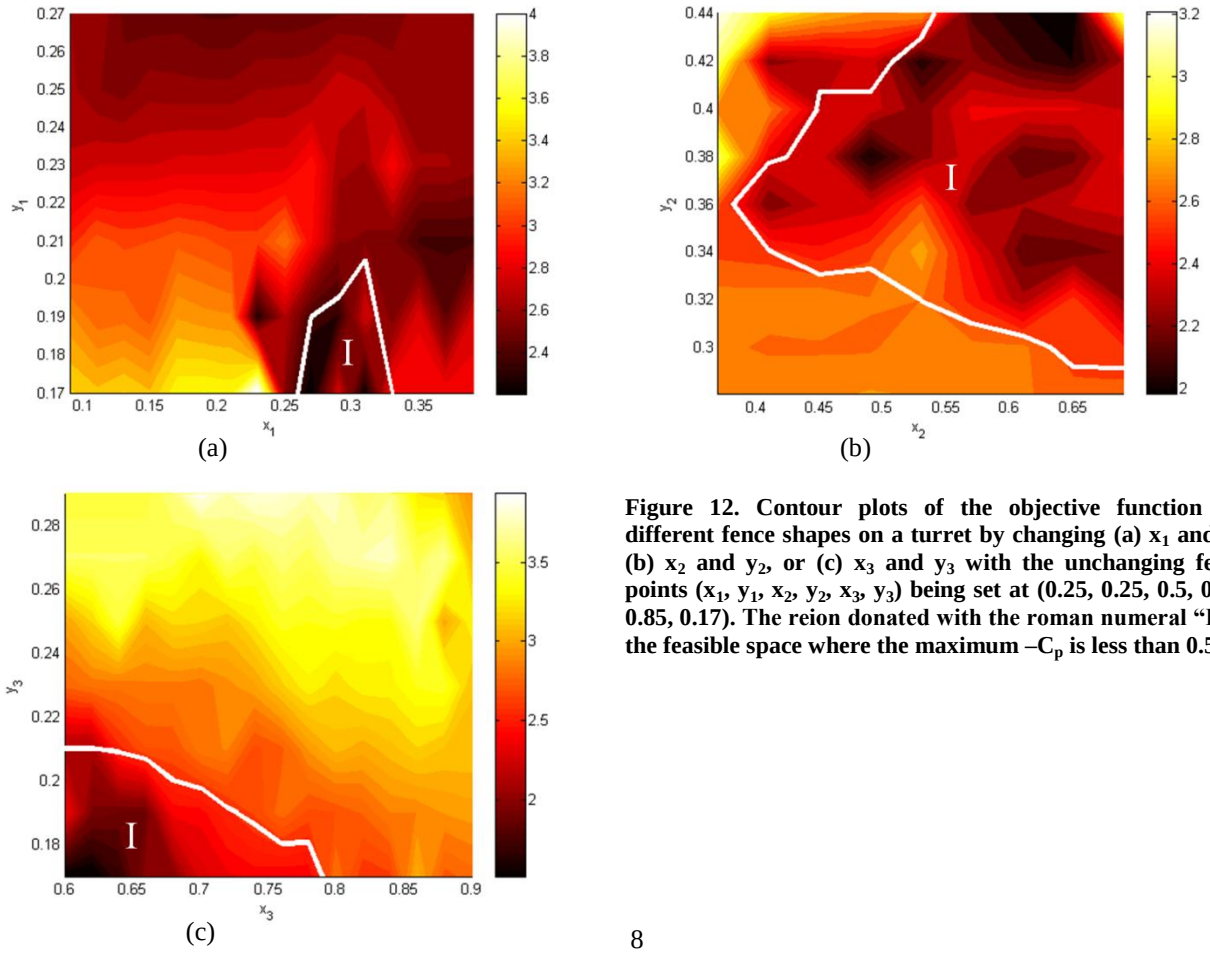

Figure 12. Contour plots of the objective function for different fence shapes on a turret by changing (a) x_1 and y_1, (b) x_2 and y_2, or (c) x_3 and y_3 with the unchanging fence points (x_1, y_1, x_2, y_2, x_3, y_3) being set at (0.25, 0.25, 0.5, 0.31, 0.85, 0.17). The reion donated with the roman numeral "I" is the feasible space where the maximum $-C_p$ is less than 0.5.

The results of this investigation are shown in Fig. 12. In Fig. 12a, (x_2, y_2, x_3, y_3) were held constant at (0.5, 0.31, 0.85, 0.17) while x_1 and y_1 were varied from 0.1 to 0.4 and 0.17 to 0.27 respectively. The white line delineates the region, denoted as region "I", where the maximum $-C_{p0}$ is under 0.5, thus fulfilling the primary constraint for the problem. Fig. 12a shows that the location of the front of the fence has a moderate influence on the objective function (i.e. the rear pressure gradient). More significantly, the small extent of the region "I" in Fig. 12a shows that there is only a limited range of positions for the front fence point that will satisfy the constraint on C_{p0}. It should be noted, however, that Fig. 12a shows the feasible range of the point 1 for only one selection of the points 2 and 3, and that a larger feasible range for the point 1 would likely result for different values of the other fence points. Furthermore, the fact that the feasible range for point 1 shown in Fig. 12a occurs at small values of *y/D* makes sense if it is noted that the fence must diffuse from point 1 to point 2 in order to maintain the C_{p0} at point 2 within the -0.5 constraint.

Figure 12b illustrates the effect that the location of the middle fence point (point 2 in Fig. 9) has on the objective function. In this case (x_1, y_1, x_3, y_3) were held constant at (0.25, 0.25, 0.85, 0.17) while x_2 and y_2 were varied from 0.37 to 0.69 and 0.28 to 0.44 respectively. Figure 12b shows that the feasible range for point 2 is significantly larger than for point 1. This result can be explained in that, for the selected locations of the points 1 and 3, there is a wide range of locations for the point 2 that will satisfy the C_{p0} criterion. In this case, the optimum location for the point 2 would be determined primarily by the minimum pressure-gradient requirement (i.e. minimization of the objective function); from Fig. 12b, this appears to occur at approximately (x_2, y_2) = (0.5, 0.38) although there are several local minima in the feasible region "I".

Figure 12c illustrates the effect that the location of the most-downstream fence point (point 3 in Fig. 9) has on the objective function. In this case (x_1, y_1, x_2, y_2) were held constant at (0.25, 0.25, 0.5, 0.31) while x_3 and y_3 were varied from 0.6 to 0.9 and 0.17 to 0.29 respectively. Figure 12c shows that the location of the point 3 has the strongest influence on the objective function (i.e., the rear pressure gradient); this result makes sense if it is recognized that point 3 determines the amount of flow contraction at the rear of the fence. The small feasible range, located at small values of y, shows that the C_{p0} criterion is also better satisfied when the point 3 is inboard of the fence point 2. Figure 12c indicates that the optimum location of the point 3 is in the vicinity of (x_3,y_3)= (0.6, 0.17).

V. Conclusion

In Rennie[5] it was shown that by adding a fence to the surface of a spherical turret, the critical Mach number could be increased while decreasing the adverse pressure gradient on the rear of the turret. In Ref. 5 the shape of the fence was determined in a trial-and-error fashion; this paper has presented the formulation of an optimization approach that will allow a systematic determination of the optimum fence shape. The optimization approach was examined over a range of reasonable fence shapes and was shown to behave in a manner that conforms to an intuitive understanding of how the fence works. In future work, the optimization technique will be improved by inclusion of a full Navier-Stokes solver, and fence shapes determined via the optimization will be tested experimentally.

References

[1]Gordeyev, S., and Jumper, E.J., "Aero-Optical Characteristics of Compressible Subsonic Turbulent Boundary Layers," AIAA-2003-3606, June 2003.

[2]Rennie, R. M., Siegenthaler, J. P., and Jumper, E. J., "Forcing of a Two-Dimensional, Weakly-Compressible Subsonic Free Shear Layer," AIAA 2006-0561, January 2006.

[3]Tyson, R.K., *Principles of Adaptive Optics*, Academic Press, Inc., San Diego, 1991.

[4] Gordeyev, S. and Jumper, E.J., "Fluid Dynamics and Aero-Optical Environment Around Turrets," AIAA Paper 2009-4224, June, 2009.

[4.1]Rennie, R. M., Duffin, D.A., and Jumper, E. J., "Characterization of a Forced Two-Dimensional, Weakly-Compressible Subsonic Free Shear Layer," AIAA 2007-4007, June 2007.

[5]Rennie, R. M., Crahan, G., and Jumper, E. J., "Aerodynamic Design of an Aircraft-Mounted Pod for Improved Aero-Optic Performance," AIAA Paper 2010-0437, January 2010.

[6]V. M. Perez, J. E. Renaud and L. T. Watson, "Interior point sequential approximate optimization methodology," In *Proceedings of the 10th AIAA/USAF/NASA/ISSMO Symposium on Multidisciplinary Analysis & Optimization*, AIAA Paper 2002-5505, September 2002.

[7]V. M. Perez, J. E. Renaud and L. T. Watson, "Reduced sampling for construction of quadratic response surface approximations using adaptive experimental design," In *Proceedings of the 43rd AIAA/ASME/ASCE/AHS/ASC Structures, Structural Dynamics, and Materials Conference*, AIAA Paper 2002-1587, April 2002.

[8]S. E. Gano, J. E. Renuad and B. Sanders, "Variable fidelity optimization using a kriging based scaling function," In *Proceedings of the 10th AIAA/ISSMO Multidisciplinary Analysis & Optimization Conference*, AIAA Paper 2004-4460, August 2004.

[9]Mejia-Rodriguez, G., J.E. Renaud, and V. Tomar, *A variable fidelity model management framework for designing multiphase materials.* J. Mechanical Design, 2008. 130(9).

[9.1]Saric, W.S., and Reshotko, E., "Review of Flow Quality Issues in Wind Tunnel Testing," AIAA Paper 1998-2613, June, 1998.

[10]Fletcher, R., "Practical Methods of Optimization," John Wiley and Sons, 1987.

[11]Gill, P.E., W. Murray, and M.H. Wright, "Numerical Linear Algebra and Optimization," Vol. 1, Addison Wesley, 1991.

[12]Powell, M.J.D., "A Fast Algorithm for Nonlinearly Constrained Optimization Calculations," Numerical Analysis, G.A.Watson ed., Lecture Notes in Mathematics, Springer Verlag, Vol. 630, 1978.